First Results from the Taiwan Axion Search Experiment with Haloscope at 19.5 μeV

Hsin Chang,[1] Jing-Yang Chang,[1] Yi-Chieh Chang,[2] Yu-Han Chang,[3] Yuan-Hann Chang,[4,5] Chien-Han Chen,[4] Ching-Fang Chen,[1] Kuan-Yu Chen,[1] Yung-Fu Chen,[1,*] Wei-Yuan Chiang,[2] Wei-Chen Chien,[3] Hien Thi Doan,[4] Wei-Cheng Hung,[1] Watson Kuo,[3] Shou-Bai Lai,[1] Han-Wen Liu,[1] Min-Wei OuYang,[1] Ping-I Wu,[1] and Shin-Shan Yu[1,5,†]

(TASEH Collaboration)

[1] *Department of Physics, National Central University, Taoyuan City 32001, Taiwan*
[2] *National Synchrotron Radiation Research Center, Hsinchu 30076, Taiwan*
[3] *Department of Physics, National Chung Hsing University, Taichung City 402, Taiwan*
[4] *Institute of Physics, Academia Sinica, Taipei City 115201, Taiwan*
[5] *Center for High Energy and High Field Physics, National Central University, Taoyuan City 32001, Taiwan*

(Dated: May 2, 2022)

This Letter reports on the first results from the Taiwan Axion Search Experiment with Haloscope, a search for axions using a microwave cavity at frequencies between 4.70750 and 4.79815 GHz. Apart from the non-axion signals, no candidates with a significance more than 3.355 were found. The experiment excludes models with the axion-two-photon coupling $|g_{a\gamma\gamma}| \gtrsim 8.2 \times 10^{-14}\,\mathrm{GeV}^{-1}$, a factor of eleven above the benchmark KSVZ model in the mass range $19.4687 < m_a < 19.8436\,\mu$eV, reaching a sensitivity three orders of magnitude better than any existing limits. It is also the first time that a haloscope-type experiment places constraints on the $g_{a\gamma\gamma}$ in this mass region.

Various astrophysical and cosmological observations indicate that dark matter (DM) exists and makes up 26.4% of the total energy density of the universe [1–5]. One of the viable dark matter candidates is the axion, which arises from the spontaneous breaking of a new global $\mathrm{U(1)_{PQ}}$ symmetry [6] introduced by Peccei and Quinn to solve the strong CP problem [6–8]. Axions are abundantly produced during the QCD phase transition in the early universe and may constitute the DM [9–12]. In the post-inflationary PQ symmetry breaking scenario, current calculations suggest a mass range of $\mathcal{O}$(1–100) μeV for axions so that the cosmic axion density does not exceed the observed cold DM density [13–25].

Axions could be detected and studied via their two-photon interaction, the so-called "inverse Primakoff effect", of which the strength is described by the coupling constant $g_{a\gamma\gamma}$. The detectors with the best sensitivities to axions with a mass of $m_a \approx \mu$eV, as first proposed by Sikivie [26, 27], are haloscopes consisting of a microwave (MW) cavity immersed in a strong static magnetic field and operated at a cryogenic temperature. In the presence of an external magnetic field, the ambient oscillating axion field drives the cavity and they resonate when the frequencies of the electromagnetic modes in the cavity match the MW frequency f, where f is set by the total energy of the axion: $hf = E_a = m_a c^2 + \frac{1}{2} m_a v^2$. The axion signal power is further delivered to the readout probe followed by a low-noise linear amplifier.

Several haloscope experiments have actively carried out axion searches, and the limits on the $g_{a\gamma\gamma}$ from a few of them have reached or approached the benchmark values. The most significant efforts are from the Axion Dark Matter eXperiment (ADMX), placing tight constraints within the mass range of 1.9–4.2 μeV [28–34]. Others include the Haloscope at Yale Sensitive to Axion Cold dark matter (HAYSTAC) [35–37], the Center for Axion and Precision Physics Research (CAPP) [38–40], and the QUest for AXions-$a\gamma$ (QUAX-$a\gamma$) [41]. This Letter presents the first results of a search for axions in the mass range of 19.4687–19.8436 μeV, from the Taiwan Axion Search Experiment with Haloscope (TASEH).

The detector of TASEH is located at the Department of Physics, National Central University, Taiwan and housed within a cryogen-free dilution refrigerator (DR) from BlueFors. An 8-Tesla superconducting solenoid with a bore diameter of 76 mm and a length of 240 mm is integrated with the DR. The DR has multiple flanges at different temperatures: 50K, 4K, still, and mixing flanges, among which the mixing flange could reach the lowest temperature at $T_{\mathrm{mx}} \simeq 27$ mK. During the data taking, the cavity sat in the center of the magnet bore and was connected via holders to the mixing flange of the DR. The 0.234-L cavity, made of oxygen-free high-conductivity (OFHC) copper, is a two-cell cylinder split along the axial direction, with an inner radius of 2.5 cm and a height of 12 cm. In order to maintain a smooth surface, the cavity underwent the processes of annealing, polishing, and chemical cleaning. The resonant frequency can be tuned via the rotation of an off-axis OFHC copper tuning rod. A readout probe, made of a 50-Ω semi-rigid coaxial cable that was soldered to an SMA (SubMiniature version A) connector, was inserted into the cavity. An additional weak-coupling probe, made of a standard SMA product, was used to inject MW sig-

* Correspondence to: yfuchen@ncu.edu.tw
† Correspondence to: syu@phy.ncu.edu.tw

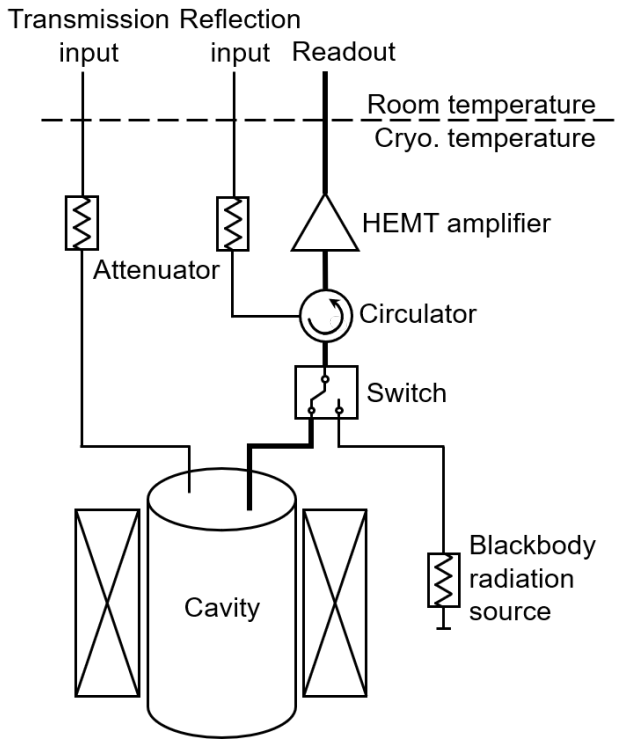

FIG. 1. The simplified diagram for the TASEH apparatus. The dashed line separates the components at room temperature and at cryogenic temperatures. The output transmission line (thick line) includes a switch, a circulator, an HEMT amplifier, and room-temperature amplifiers. Via the cryogenic switch, the output line can also be connected to a blackbody radiation source, made of a 50-Ω terminator, for calibration of the amplification chain. The two input lines, used to inject MW signals, have one attenuator thermally anchored at each cold flange to reduce the broadband radiation from the higher-temperature environment or flanges.

nals for examining the cavity characteristics and for testing the signal receivers. The signal from the readout probe was directed to an impedance-matched amplification chain. The first-stage amplifier was a low noise high-electron-mobility transistor (HEMT) amplifier mounted on the 4K flange. A three-stage circulator was anchored at the mixing flange to prevent thermal radiation from the HEMT amplifier back streaming to the cold cavity and then being reflected. The signal was further amplified at room temperature via a three-stage post-amplifier, and down-converted and demodulated to in-phase (I) and quadrature (Q) components and digitized by an analog-to-digital converter with a sampling rate of 2 MHz. Figure 1 shows a simplified diagram for the TASEH apparatus. More details of the TASEH detector can be found in Ref. [42].

The signal power extracted from a MW cavity on resonance is given by [35, 43]:

$$P_s = \left(g_\gamma^2 \frac{\alpha^2 \hbar^3 c^3 \rho_a}{\pi^2 \Lambda^4}\right) \times \left(\omega_c \frac{1}{\mu_0} B_0^2 V C Q_L \frac{\beta}{1+\beta}\right). \quad (1)$$

The first set of parentheses contains physical constants, a dimensionless model-dependent parameter g_γ, and the local dark-matter density $\rho_a = 0.45$ GeV/cm^3 [5, 44]. The numerical values of g_γ are -0.97 and 0.36 in the Kim-Shifman-Vainshtein-Zakharov (KSVZ) [45, 46] and the Dine-Fischler-Srednicki-Zhitnitsky (DFSZ) [47, 48] benchmark models, respectively. For the QCD axions, the $g_{a\gamma\gamma}$ is related to g_γ and the axion mass m_a:

$$g_{a\gamma\gamma} = \left(\frac{g_\gamma \alpha}{\pi \Lambda^2}\right) m_a, \quad (2)$$

where α is the fine-structure constant and $\Lambda = 78$ MeV is a scale parameter that can be derived from the mass and the decay constant of the pion and the ratio of the up to down quark masses. The second set of parentheses contains parameters related to the experimental setup: the angular resonant frequency of the cavity ω_c, the vacuum permeability μ_0, the nominal strength of the external magnetic field B_0, the effective volume of the cavity V, and the loaded quality factor of the cavity $Q_L = Q_0/(1+\beta)$, where Q_0 is the unloaded, intrinsic quality factor and β is the coupling coefficient which determines the amount of coupling of the signal to the receiver. The form factor C is the normalized overlap of the electric field $\vec{\boldsymbol{E}}$, for a particular cavity resonant mode, with the external magnetic field $\vec{\boldsymbol{B}}$:

$$C = \frac{\left[\int \left(\vec{\boldsymbol{B}} \cdot \vec{\boldsymbol{E}}\right) d^3\boldsymbol{x}\right]^2}{B_0^2 V \int E^2 d^3\boldsymbol{x}}. \quad (3)$$

The magnetic field $\vec{\boldsymbol{B}}$ in TASEH points mostly along the axial direction of the cavity, with a small variation of field strength along the radial and axial directions. For cylindrical cavities, the largest form factor is from the TM_{010} mode. The expected signal power derived from the experimental parameters of TASEH is $P_s \simeq 1.4 \times 10^{-24}$ W for a KSVZ axion with a mass of 19.5 μeV.

In the axion experiments, the figure of merit that determines the design of the experimental setup is the signal-to-noise ratio (SNR), i.e. the ratio of the signal power P_s to the fluctuation in the averaged noise power spectrum σ_n. According to Dicke's Radiometer Equation [49], the σ_n is given by:

$$\sigma_n = k_B T_{\rm sys} \sqrt{\frac{\Delta f}{t}} \quad (4)$$

where $T_{\rm sys}$ is the system noise temperature, an effective temperature associated with the total noise of the system, t is the data integration time t and Δf is the resolution

bandwidth. Assuming that all the axion signal power falls within Δf, the SNR will therefore be:

$$\mathrm{SNR} = \frac{P_s}{\sigma_n} = \frac{P_s}{k_B T_{\mathrm{sys}}}\sqrt{\frac{t}{\Delta f}}. \tag{5}$$

The system noise temperature T_{sys} has three major components:

$$T_{\mathrm{sys}} = \tilde{T}_{\mathrm{mx}} + \left(\tilde{T}_{\mathrm{c}} - \tilde{T}_{\mathrm{mx}}\right) L(\omega) + T_{\mathrm{a}}, \tag{6}$$

where ω is the angular frequency. The last term T_{a} is the effective temperature of the noise added by the receiver (mainly from the first-stage amplifier). The sum of the first two terms is equivalent to the sum of the reflection of the incoming noise from the attenuator anchored to the mixing flange and the transmission of the noise from the cavity body itself. The $\tilde{T}_i = \left(\frac{1}{e^{\hbar\omega/k_B T_i}-1} + \frac{1}{2}\right)\hbar\omega/k_B$ refers to the effective temperature due to the blackbody radiation at a physical temperature T_i and the vacuum fluctuation. The difference of the effective temperatures $\tilde{T}_{\mathrm{c}} - \tilde{T}_{\mathrm{mx}}$ is modulated by a Lorentzian function $L(\omega)$. If the physical temperature of the cavity T_{c} and T_{mx} were identical, the thermal noise spectrum from the cavity would be white. The derivation of the first two terms in Eq. (6) can be found in Ref. [50]. The T_{a} obtained from the calibration via the blackbody radiation source in Fig. 1 is about $1.9 - 2.2$ K and the baseline value of T_{sys} is about 2.0–2.3 K.

The data for the analysis presented here were collected by TASEH from October 13, 2021 to November 15, 2021, and are termed as the CD102 data, where CD stands for "cool down". The CD102 data cover the frequency range of 4.70750–4.79815 GHz. In this Letter, most of the frequencies in unit of GHz are quoted with five decimal places as the absolute accuracy of frequency is ≈ 10 kHz. It shall be noted that the frequency resolution is 1 kHz. During the CD102 data run, the temperature of the cavity stayed at $T_{\mathrm{c}} \simeq 155$ mK, higher with respect to the mixing flange; it is believed that the cavity had an unexpected thermal contact with the radiation shield in the DR. The form factor C for the TM_{010} mode varies from 0.60 to 0.61 over the operational frequency range. The Q_0 at the cryogenic temperature ($T_{\mathrm{c}} \simeq 155$ mK) is $\simeq 60700$. There were 837 resonant-frequency steps in total, with a frequency difference of $\Delta f_{\mathrm{s}} = 95 - 115$ kHz between the steps. The value of Δf_{s} was kept within 10% of 105 kHz rather than a fixed value, such that the rotation angle of the tuning rod did not need to be fine-tuned and the operation time could be minimized; a 10% variation of the Δf_{s} is found to have no impact on the $|g_{a\gamma\gamma}|$ limits. Each resonant-frequency step is denoted as a "scan" and the data integration time was about 32-42 minutes. The integration time was determined based on the target $|g_{a\gamma\gamma}|$ limits and the experimental parameters; the variation of the integration time aimed to remove the frequency-dependence in the $|g_{a\gamma\gamma}|$ limits caused by frequency dependence of the added noise T_{a}. The depth of the readout probe was set for $\beta \simeq 2$ since this value maximizes the scan rate, namely the coverage of frequency scans for a given amount of time.

The analysis of the TASEH CD102 data follows the procedure similar to that developed by the HAYSTAC experiment [51] and the details are described in Ref. [50]. The fast Fourier transform (FFT) algorithm is performed on the IQ time series data to obtain the frequency-domain power spectrum. The Savitzky-Golay (SG) filter [52] is applied to remove the Lorentzian structure of the background caused by the temperature difference between the cavity and the mixing flange [Eq. (6)]. All the spectra from different frequency scans, particularly for the frequency bins that appear in multiple spectra, are combined with a weighting algorithm. The uncertainty of the averaged power at the overlapped region is reduced due to the combination. In order to maximize the SNR, a running window of five consecutive bins in the combined spectrum is applied and the five bins within each window are merged to construct a final spectrum. The five frequency bins correspond to the 5-kHz axion signal line width, derived from the standard assumption of axion signal line shape as described by Eq. (7). This signal line shape is also used when defining the maximum likelihood weights for merging:

$$\mathcal{F}(f, f_a) = \frac{2}{\sqrt{\pi}}\sqrt{f - f_a}\left(\frac{3}{\alpha}\right)^{3/2} e^{\frac{-3(f-f_a)}{\alpha}}, \tag{7}$$

where $\alpha \equiv f_a \left\langle v^2 \right\rangle / c^2$. Here, the frequency f must be greater or equal to the axion frequency $f_a = m_a c^2/h$. In this standard assumption of axion signal line shape, the DM halo density distribution is assumed to be spherically symmetric and close to be isothermal, which results in a velocity distribution similar to the Maxwell-Boltzmann distribution. Therefore, the variance $\left\langle v^2 \right\rangle$ and the most probable velocity (speed) v_p are related to each other: $\left\langle v^2 \right\rangle = 3v_p^2/2 = (270\ \mathrm{km/s})^2$, where $v_p = 220$ km/s is the local circular velocity of DM in the galactic rest frame and this value is also used by other axion experiments.

After the merging, if there were any potential signal with an SNR larger than 3.355, a rescan would be proceeded to check if it were a real signal or a statistical fluctuation. The procedure of the CD102 data taking was to perform a rescan after covering every 10 MHz; the rescan was done by adjusting the tuning rod of the cavity so to match the resonant frequency to the frequency of the candidate. In total, 22 candidates with an SNR greater than 3.355 were found. Among them, 10 candidates were from the fluctuations because they were gone after a few rescans. The remaining two candidates, in the frequency ranges of 4.71017 – 4.71019 GHz and 4.74730 – 4.74738 GHz, are excluded from consideration of axion signal candidates. The signal in the second frequency

range was detected via a portable antenna outside the DR and found to come from the instrument control computer in the laboratory, while the signal in the first frequency range was not detected outside the DR but still present after turning off the external magnetic field. Therefore, no limits are placed for the above two frequency ranges.

Since no candidates were found after the rescan, the upper limits at 95% confidence level (C.L.) on the $|g_\gamma|$ and the $|g_{a\gamma\gamma}|$ are derived by setting the maximum SNR equal to five. Figure 2 shows the limits on the $|g_{a\gamma\gamma}|$ from TASEH and the ratio of the limits on the $|g_\gamma|$ with respect to the KSVZ benchmark value ($|g_{\rm KSVZ}| = 0.97$) from TASEH together with those from the previous searches. The limits on $|g_{a\gamma\gamma}|$ range from $5.3\times10^{-14}\,\mathrm{GeV}^{-1}$ to $8.9\times10^{-14}\,\mathrm{GeV}^{-1}$, with an average value of $8.2\times10^{-14}\,\mathrm{GeV}^{-1}$; the lowest value comes from the frequency bins with additional eight times more data from the rescans, while the highest value comes from the frequency bins near the boundaries of the spectrum. The analysis that merges bins without assuming a signal line shape results in $\approx 5.5\%$ larger values on the $|g_{a\gamma\gamma}|$ limits. If a Gaussian signal line shape with an FWHM of 2.5 kHz, about half of the axion line width in Eq. (7), is assumed instead, the limits will be $\approx 3.8\%$ smaller than the central results. If the $|g_{a\gamma\gamma}|$ limits are derived from the observed SNR as described in the ADMX paper [53], rather than using the 5σ target SNR, the average limit on $|g_{a\gamma\gamma}|$ will be $\approx 4.9\times10^{-14}\,\mathrm{GeV}^{-1}$. Overall the total relative systematic uncertainty is $\approx 4.6\%$, coming from the uncertainties on the loaded quality factor Q_L, the coupling coefficient β, the added noise temperature $T_{\rm a}$, the effect of the misalignment between the true axion frequency and the lower boundaries of the frequency bins, and the variation of the SG-filter parameters.

After the collection of the CD102 data, the synthetic axion signals were injected into the cavity and read out via the same transmission line and amplification chain. The procedure to generate axion-like signals is summarized in Ref. [42] and the analysis of the synthetic axion data is described in Ref. [50]. The analysis results of the synthetic axion signals demonstrates the capability of the experimental setup and the analysis strategy to discover an axion signal with $|g_\gamma| \approx \mathcal{O}\left(10\,|g_{\rm KSVZ}|\right)$.

This Letter presents the first results of a search for axions for the mass range $19.4687 < m_a < 19.8436\,\mu$eV. Apart from the non-axion signals, no candidates with a significance more than 3.355 were found. The experiment excludes models with the axion-two-photon coupling $|g_{a\gamma\gamma}| \gtrsim 8.2\times10^{-14}\,\mathrm{GeV}^{-1}$ at 95% C.L., a factor of eleven above the benchmark KSVZ model. The sensitivity on $|g_{a\gamma\gamma}|$ reached by TASEH is three orders of magnitude better than the existing limits. It is also the first time that a haloscope-type experiment places constraints in this mass region.

We thank Chao-Lin Kuo for his help to initiate this project as well as discussions on the microwave cavity design, Gray Rybka and Nicole Crisosto for their introduction of the ADMX experimental setup and analysis, Anson Hook for the discussions and the review of the axion theory, and Jiunn-Wei Chen, Cheng-Wei Chiang, Cheng-Pang Liu, and Asuka Ito for the discussions of future improvements in axion searches. The work of the TASEH Collaboration was funded by the Ministry of Science and Technology (MoST) of Taiwan with grant numbers MoST-109-2123-M-001-002, MoST-110-2123-M-001-006, MoST-110-2112-M-213-018, MoST-110-2628-M-008-003-MY3, and MoST-109-2112-M-008-013-MY3, and by the Institute of Physics, Academia Sinica.

[1] R. J. Gaitskell, Ann. Rev. Nucl. Part. Sci. **54**, 315 (2004).
[2] V. Trimble, Ann. Rev. Astron. Astrophys. **25**, 425 (1987).
[3] T. A. Porter, R. P. Johnson, and P. W. Graham, Ann. Rev. Astron. Astrophys. **49**, 155 (2011).
[4] N. Aghanim *et al.* (Planck), Astron. Astrophys. **641**, A6 (2020), [Erratum: Astron.Astrophys. 652, C4 (2021)].
[5] P. A. Zyla *et al.* (Particle Data Group), PTEP **2020**, 083C01 (2021).
[6] R. D. Peccei and H. R. Quinn, Phys. Rev. Lett. **38**, 1440 (1977).
[7] S. Weinberg, Phys. Rev. Lett. **40**, 223 (1978).
[8] F. Wilczek, Phys. Rev. Lett. **40**, 279 (1978).
[9] J. Preskill, M. B. Wise, and F. Wilczek, Physics Letters B **120**, 127 (1983).
[10] L. Abbott and P. Sikivie, Physics Letters B **120**, 133 (1983).
[11] M. Dine and W. Fischler, Physics Letters B **120**, 137 (1983).
[12] J. Ipser and P. Sikivie, Phys. Rev. Lett. **50**, 925 (1983).
[13] S. Borsanyi, Z. Fodor, J. Guenther, K.-H. Kampert, S. D. Katz, T. Kawanai, T. G. Kovacs, S. W. Mages, A. Pasztor, F. Pittler, J. Redondo, A. Ringwald, and K. K. Szabo, Nature **539**, 69 (2016).
[14] M. Dine, P. Draper, L. Stephenson-Haskins, and D. Xu, Phys. Rev. D **96**, 095001 (2017).
[15] T. Hiramatsu, M. Kawasaki, T. Sekiguchi, M. Yamaguchi, and J. Yokoyama, Phys. Rev. D **83**, 123531 (2011).
[16] M. Kawasaki, K. Saikawa, and T. Sekiguchi, Phys. Rev. D **91**, 065014 (2015).
[17] E. Berkowitz, M. I. Buchoff, and E. Rinaldi, Phys. Rev. D **92**, 034507 (2015).
[18] L. Fleury and G. D. Moore, J. Cosmol. Astropart. Phys. **01** (2016), 004.
[19] C. Bonati, M. D'Elia, M. Mariti, G. Martinelli, M. Mesiti, F. Negro, F. Sanfilippo, and G. Villadoro, JHEP **03** (2016), 155.
[20] P. Petreczky, H.-P. Schadler, and S. Sharma, Phys. Lett. B **762**, 498 (2016).
[21] G. Ballesteros, J. Redondo, A. Ringwald, and C. Tamarit, Phys. Rev. Lett. **118**, 071802 (2017).
[22] V. B. Klaer and G. D. Moore, J. Cosmol. Astropart. Phys. **11** (2017), 049.
[23] M. Buschmann, J. W. Foster, and B. R. Safdi, Phys. Rev. Lett. **124**, 161103 (2020).
[24] M. Gorghetto, E. Hardy, and G. Villadoro, SciPost Phys.

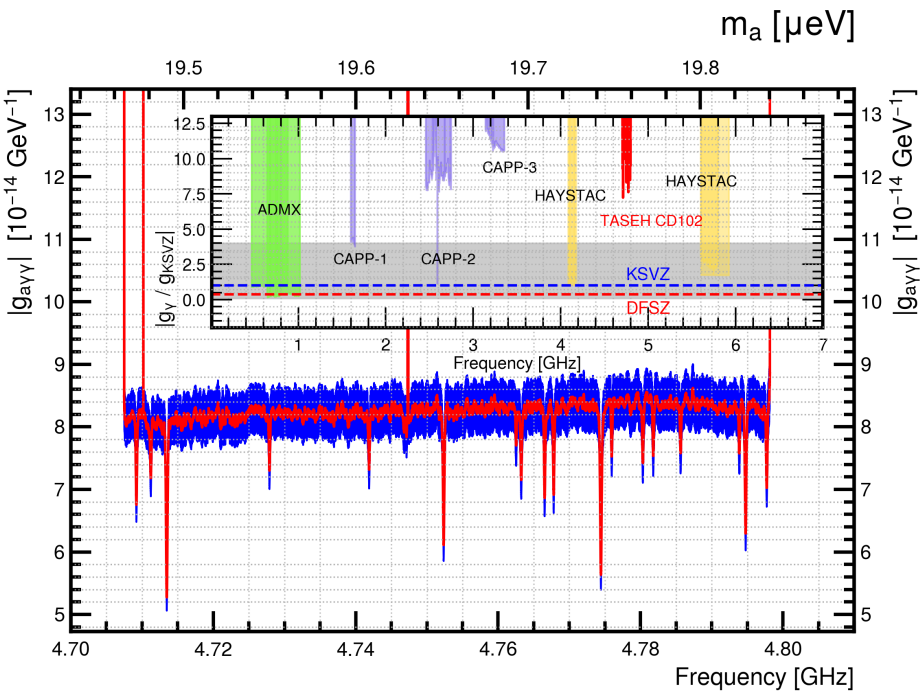

FIG. 2. The 95% C.L. limits on $|g_{a\gamma\gamma}|$ from TASEH and the ratio of the limits on $|g_\gamma|$ with respect to the benchmark value $|g_{\rm KSVZ}|$ from the CD102 data of TASEH (red band) and previous searches performed by the ADMX, CAPP, and HAYSTAC Collaborations (inset). The blue error band indicates the systematic uncertainties. The gray band in the inset shows the allowed region of $|g_\gamma|$ vs. m_a from various QCD axion models, while the blue and red dashed lines are the values predicted by the KSVZ and DFSZ benchmark models, respectively.

10, 050 (2021).

[25] M. Buschmann, J. W. Foster, A. Hook, A. Peterson, D. E. Willcox, W. Zhang, and B. R. Safdi, Nature Commun. **13**, 1049 (2022).

[26] P. Sikivie, Phys. Rev. Lett. **51**, 1415 (1983).

[27] P. Sikivie, Phys. Rev. D **32**, 2988 (1985).

[28] C. Hagmann, D. Kinion, W. Stoeffl, K. van Bibber, E. Daw, H. Peng, L. J. Rosenberg, J. LaVeigne, P. Sikivie, N. S. Sullivan, D. B. Tanner, F. Nezrick, M. S. Turner, D. M. Moltz, J. Powell, and N. A. Golubev, Phys. Rev. Lett. **80**, 2043 (1998).

[29] S. J. Asztalos, E. Daw, H. Peng, L. J. Rosenberg, D. B. Yu, C. Hagmann, D. Kinion, W. Stoeffl, K. van Bibber, J. LaVeigne, P. Sikivie, N. S. Sullivan, D. B. Tanner, F. Nezrick, and D. M. Moltz, The Astrophysical Journal **571**, L27 (2002).

[30] S. J. Asztalos, R. F. Bradley, L. Duffy, C. Hagmann, D. Kinion, D. M. Moltz, L. J. Rosenberg, P. Sikivie, W. Stoeffl, N. S. Sullivan, D. B. Tanner, K. van Bibber, and D. B. Yu, Phys. Rev. D **69**, 011101 (R) (2004).

[31] S. J. Asztalos, G. Carosi, C. Hagmann, D. Kinion, K. van Bibber, M. Hotz, L. J. Rosenberg, G. Rybka, J. Hoskins, J. Hwang, P. Sikivie, D. B. Tanner, R. Bradley, and J. Clarke, Phys. Rev. Lett. **104**, 041301 (2010).

[32] N. Du *et al.* (ADMX Collaboration), Phys. Rev. Lett. **120**, 151301 (2018).

[33] T. Braine *et al.* (ADMX Collaboration), Phys. Rev. Lett. **124**, 101303 (2020).

[34] C. Bartram *et al.* (ADMX Collaboration), Phys. Rev. Lett. **127**, 261803 (2021).

[35] B. M. Brubaker, L. Zhong, Y. V. Gurevich, S. B. Cahn, S. K. Lamoreaux, M. Simanovskaia, J. R. Root, S. M. Lewis, S. Al Kenany, K. M. Backes, I. Urdinaran, N. M. Rapidis, T. M. Shokair, K. A. van Bibber, D. A. Palken, M. Malnou, W. F. Kindel, M. A. Anil, K. W. Lehnert, and G. Carosi, Phys. Rev. Lett. **118**, 061302 (2017).

[36] L. Zhong, S. Al Kenany, K. M. Backes, B. M. Brubaker, S. B. Cahn, G. Carosi, Y. V. Gurevich, W. F. Kindel, S. K. Lamoreaux, K. W. Lehnert, S. M. Lewis, M. Malnou, R. H. Maruyama, D. A. Palken, N. M. Rapidis, J. R. Root, M. Simanovskaia, T. M. Shokair, D. H. Speller, I. Urdinaran, and K. A. van Bibber, Phys. Rev. D **97**, 092001 (2018).

[37] K. M. Backes, D. A. Palken, S. Al Kenany, B. M. Brubaker, S. B. Cahn, A. Droster, G. C. Hilton, S. Ghosh, H. Jackson, S. K. Lamoreaux, A. F. Leder, K. W. Lehnert, S. M. Lewis, M. Malnou, R. H. Maruyama, N. M. Rapidis, M. Simanovskaia, S. Singh, D. H. Speller, I. Urdinaran, L. R. Vale, E. C. van Assendelft, K. van Bibber, and H. Wang, Nature **590**, 238–242 (2021).

[38] S. Lee, S. Ahn, J. Choi, B. R. Ko, and Y. K. Semertzidis, Phys. Rev. Lett. **124**, 101802 (2020).

[39] J. Jeong, S. Youn, S. Bae, J. Kim, T. Seong, J. E. Kim, and Y. K. Semertzidis, Phys. Rev. Lett. **125**, 221302 (2020).

[40] O. Kwon, D. Lee, W. Chung, D. Ahn, H. Byun, F. Caspers, H. Choi, J. Choi, Y. Chong, H. Jeong,

J. Jeong, J. E. Kim, J. Kim, C. Kutlu, J. Lee, M. Lee, S. Lee, A. Matlashov, S. Oh, S. Park, S. Uchaikin, S. Youn, and Y. K. Semertzidis, Phys. Rev. Lett. **126**, 191802 (2021).

[41] D. Alesini, C. Braggio, G. Carugno, N. Crescini, D. D'Agostino, D. Di Gioacchino, R. Di Vora, P. Falferi, U. Gambardella, C. Gatti, G. Iannone, C. Ligi, A. Lombardi, G. Maccarrone, A. Ortolan, R. Pengo, A. Rettaroli, G. Ruoso, L. Taffarello, and S. Tocci, Phys. Rev. D **103**, 102004 (2021).

[42] H. Chang, J.-Y. Chang, Y.-C. Chang, Y.-H. Chang, Y.-H. Chang, C.-H. Chen, C.-F. Chen, K.-Y. Chen, Y.-F. Chen, W.-Y. Chiang, W.-C. Chien, H. T. Doan, W.-C. Hung, W. Kuo, S.-B. Lai, H.-W. Liu, M.-W. OuYang, P.-I. Wu, and S.-S. Yu (TASEH Collaboration), (2022), arXiv:2205.xxxx [physics.ins-det].

[43] D. Alesini, C. Braggio, G. Carugno, N. Crescini, D. D'Agostino, D. Di Gioacchino, R. Di Vora, P. Falferi, S. Gallo, U. Gambardella, C. Gatti, G. Iannone, G. Lamanna, C. Ligi, A. Lombardi, R. Mezzena, A. Ortolan, R. Pengo, N. Pompeo, A. Rettaroli, G. Ruoso, E. Silva, C. C. Speake, L. Taffarello, and S. Tocci, Phys. Rev. D **99**, 101101 (2019).

[44] J. I. Read, J. Phys. G: Nucl. Part. Phys. **41**, 063101 (2014). Both 0.45 GeV/cm^3 (used by ADMX, HAYSTAC, CAPP, and QUAX-$a\gamma$) and 0.3 GeV/cm^3 (more commonly cited by the other direct DM search experiments) are consistent with the recent measurements.

[45] J. E. Kim, Phys. Rev. Lett. **43**, 103 (1979).

[46] M. A. Shifman, A. I. Vainshtein, and V. I. Zakharov, Nucl. Phys. B **166**, 493 (1980).

[47] M. Dine, W. Fischler, and M. Srednicki, Phys. Lett. B **104**, 199 (1981).

[48] A. R. Zhitnitsky, Sov. J. Nucl. Phys. **31**, 260 (1980).

[49] R. H. Dicke, Review of Scientific Instruments **17**, 268 (1946).

[50] H. Chang, J.-Y. Chang, Y.-C. Chang, Y.-H. Chang, Y.-H. Chang, C.-H. Chen, C.-F. Chen, K.-Y. Chen, Y.-F. Chen, W.-Y. Chiang, W.-C. Chien, H. T. Doan, W.-C. Hung, W. Kuo, S.-B. Lai, H.-W. Liu, M.-W. OuYang, P.-I. Wu, and S.-S. Yu (TASEH Collaboration), (2022), arXiv:2204.14265 [hep-ex].

[51] B. M. Brubaker, L. Zhong, S. K. Lamoreaux, K. W. Lehnert, and K. A. van Bibber, Phys. Rev. D **96**, 123008 (2017).

[52] A. Savitzky and M. J. E. Golay, Anal. Chem. **36**, 1627 (1964).

[53] C. Bartram *et al.* (ADMX Collaboration), Phys. Rev. D **103**, 032002 (2021).